NACA

RESEARCH MEMORANDUM

SUPERSONIC-AREA-RULE DESIGN AND ROCKET-PROPELLED FLIGHT INVESTIGATION OF A ZERO-LIFT STRAIGHT-WING—BODY—NACELLE CONFIGURATION BETWEEN MACH NUMBERS 0.8 AND 1.53

By Sherwood Hoffman

Langley Aeronautical Laboratory
Langley Field, Va.

CLASSIFIED DOCUMENT

NATIONAL ADVISORY COMMITTEE
FOR AERONAUTICS

WASHINGTON
April 26, 1956

Unclassified

NASA Tech Pub Announcement

TO CHANGE)

26 Aug 59

NK

G CHANGE)

9 Mar 61

DATE

NATIONAL ADVISORY COMMITTEE FOR AERONAUTICS

RESEARCH MEMORANDUM

SUPERSONIC-AREA-RULE DESIGN AND ROCKET-PROPELLED FLIGHT INVESTIGATION OF A ZERO-LIFT STRAIGHT-WING—BODY—NACELLE CONFIGURATION BETWEEN MACH NUMBERS 0.8 AND 1.53

By Sherwood Hoffman

SUMMARY

The supersonic-area-rule concept was applied to the design of a straight-wing—body combination with large symmetrically mounted nacelles located at the 70-percent-semispan station. Both the nacelles and fuselage were indented to give a smooth total area distribution at a design Mach number of 1.41. The model was a zero-lift rocket-propelled vehicle and covered a continuous range of Mach number from 0.8 to 1.53 with corresponding Reynolds number from 3×10^6 to 4×10^6, based on wing mean aerodynamic chord. Also tested were two small equivalent bodies of revolution for Mach number 1.0 (which were propelled from a helium gun) of the basic wing-body combination.

The pressure drag from the configuration with nacelles was significantly less than that from a corresponding configuration without nacelles throughout the Mach number range. Both configurations were designed to have the same average area distribution at Mach number 1.41. The moment-of-area rule was useful in explaining the relative drag rises of the models at low supersonic speeds.

The pressure drag from the Mach number 1.0 equivalent bodies of revolution compared favorably with that from the corresponding straight-wing—body configuration between the drag-rise Mach number and the speed of sound.

INTRODUCTION

This paper presents the results of an application of the supersonic area rule (ref. 1) to the design of a straight-wing—body configuration with large nacelles. Previous applications of the area-rule concept to

configurations with external installations were made for design Mach numbers near 1.0 utilizing the transonic area rule (ref. 2) and the moment-of-area rule (ref. 3). These investigations are listed with other interesting area-rule investigations in references 1 to 20.

The configuration was designed to have a smooth average area distribution at Mach number 1.41. The wing had an aspect ratio of 3.04, taper ratio 0.394, 0° of sweep along the 75-percent chord line, and an NACA 65A004.5 airfoil section in the free-stream direction. The nacelles were twice as long as the wing mean aerodynamic chord, had a mass-flow ratio of 1.0, and were symmetrically mounted at the 70-percent-semispan station of the wing. Both the nacelles and fuselage were contoured to give the desired average area distribution.

Also presented herein is the test result of a Mach number 1.0 equivalent body-of-revolution of the basic wing-body combination used for the aforementioned design study.

The models were flight tested at the Langley Pilotless Aircraft Research Station at Wallops Island, Va. Zero-lift drag measurements were obtained for the model with nacelles through a Mach number range from 0.8 to 1.53 and corresponding Reynolds number range from 3×10^6 to 4×10^6, based on wing mean aerodynamic chord. The equivalent body models were tested at transonic speeds at an average Reynolds number of 1.2×10^6.

SYMBOLS

A	cross-sectional area
a	tangential acceleration
C_D	total drag coefficient, based on S_w
ΔC_D	pressure-drag coefficient, based on S_w
C_{D_f}	friction-drag coefficient, based on S_w
$\bar{c}$	mean aerodynamic chord of wing
d	maximum diameter of equivalent body revolution
g	acceleration due to gravity
l	length of fuselage

l_2	length of second moment-of-area distribution of wing alone or wing with nacelles
M	Mach number
$M_2(x)$	second moment-of-area distribution of wing alone or wing with nacelles normal to the axis of symmetry
q	free-stream dynamic pressure
R	Reynolds number, based on $\bar{c}$
S_W	total wing plan-form area
W	weight of model during deceleration
x	longitudinal station
γ	angle between flight path and horizontal

MODELS

Details and dimensions of the models tested and of two reference models are given in figure 1 and tables I to VI. Photographs and area distributions of the models are presented in figures 2 and 3, respectively.

The wing-body-nacelle configuration (model A) was designed to have a smooth average area distribution at Mach number 1.41 (fig. 3(b)) by using Faget's method of hoops (ref. 5). The wing had an aspect ratio of 3.04, taper ratio of 0.394, 0° of sweep along the 75-percent-chord line, and an NACA 65A004.5 airfoil section in the free-stream direction. The contoured nacelles had a fineness ratio of 7.83, were designed for a mass-flow ratio 1.0, and were symmetrically mounted on the wings at the 70-percent-semispan station. The duct of the nacelle was cylindrical with a sharp lip at the inlet. The contoured fuselage was a body of revolution of fineness ratio 10.9.

For the present design application, the cross-sectional-area distribution of a parabolic body of revolution of fineness ratio 10 (table V) was selected for the desired average area distribution at $M = 1.41$ and for the basic fuselage of the model. The nacelles were designed to be long (twice length of $\bar{c}$) and, before contouring, with a long cylindrical midsection to give a uniform distribution of cross-sectional area. The nacelles were indented symmetrically in order to cancel the average projected wing areas intercepted by the Mach planes between the wing tips and outer edges of the nacelles. This modification was designed on the

premise that such an indentation would be more effective than a corresponding fuselage indentation for reducing the local interference between the wing tip and nacelle. The fuselage was indented accordingly in order to cancel the remaining wing and nacelle sectional areas. Thus the wing sectional areas were cancelled at three spanwise stations corresponding to the root chord and the 70-percent-semispan station on each wing panel. The nacelle inlet area was subtracted from the nacelle cross-sectional areas to allow for internal flow. No area adjustments were made for the thin stabilizing fins of the model.

The two reference configurations (models B and C) utilized the same wing as the present configuration without the nacelles. Model B was indented for the wing at $M = 1.41$ (ref. 5) and model C represents the basic configuration with the original parabolic fuselage (ref. 21).

Models D and E were duplicate equivalent bodies of revolution (for $M = 1.0$) of the basic configuration model C.

TESTS AND MEASUREMENTS

All the models were tested at the Langley Pilotless Aircraft Research Station at Wallops Island, Va. The three wing-body configurations presented herein were zero-lift rocket-propelled models that were accelerated from zero-length launchers to supersonic speeds. Model A, which was designed for this investigation, was propelled by a fin-stabilized 6-inch ABL Deacon rocket motor booster (fig. 2(c)) that separated from the model after burnout. The equivalent body models D and E were propelled from the helium gun which is described in reference 19. Velocity and trajectory data were obtained from the CW Doppler velocimeter and the NACA modified SCR 584 tracking radar unit, respectively. A survey of atmospheric conditions including winds aloft was made by radiosonde measurements from an ascending balloon that was released at the time of each launching.

The flight tests covered continuous ranges of Mach numbers varying between 0.8 and 1.53. The corresponding Reynolds numbers, based on wing mean aerodynamic chord, are shown in figure 4 to vary from approximately 3×10^6 to 4×10^6 for model A, 5×10^6 to 13×10^6 for model B, $9 = 10^6$ to 25×10^6 for model C, and from 1×10^6 to 2×10^6 for models D and E through the Mach number ranges covered.

The values of total drag coefficient, based on total wing plan-form area, for all the models were obtained during decelerating flight with the expression

$$C_D = -\frac{W}{qgS_w}(a + g \sin \gamma)$$

where a was obtained by differentiating the velocity-time curve from the CW Doppler velocimeter. A more complete method of reducing the data is given in reference 22.

The pressure-drag or drag-rise coefficient ΔC_D for model A was obtained by subtracting the friction drag, fin drag (ref. 5), and the estimated internal drag of the nacelles from the total drag coefficient through the Mach number range. The friction-drag coefficient was determined for the Reynolds number range by adjusting the subsonic drag level for Reynolds number effect by using average Reynolds numbers and Van Driest's turbulent-friction coefficients for flat plates (ref. 23). The internal pressure drag of the nacelles was estimated by computing the momentum loss for the entering stream tube assuming a normal shock at the inlet and a mass-flow ratio of 1.0. The pressure drag was not corrected for base drag rise; however, reference 21 indicates that the base drag rise was of the order of 0.001 based on wing area. The same procedure was used in determining the pressure drags of the two reference configurations (models B and C) using the basic data published in references 5 and 21, respectively, and for the two equivalent bodies of revolution (models D and E).

The error in total drag coefficient was estimated to be approximately ± 0.0007 at supersonic speeds and ± 0.001 at transonic speeds. The Mach numbers were determined within ± 0.01 throughout the test range.

RESULTS AND DISCUSSION

The variations of total drag coefficient, friction-drag coefficient, and fin-drag coefficient with Mach number for models A, B, and C and the estimated internal drag of the two nacelles, based on total wing planform area, are presented in figure 5(a). It is not possible to determine the nacelle drag increments accurately from the tests because of the different body indentations used on models A and B. At Mach number 0.8, the drag increment between models A and B is almost entirely accounted for by skin friction and the different test Reynolds numbers. Approximately 85 percent of this increment results from the internal and external friction drag of the large nacelles, about 10 percent results from increasing friction drag due to the change in body surface area from fuselage contouring, and 5 percent is due to the Reynolds number difference. According to these calculations, it appears that little or no local interference was obtained at high subsonic speeds by changing the body shape or possibly by indenting the nacelles. At $M = 1.5$, the incremental drag difference between models A and B is much less than at Mach number 0.8. This indicates large favorable interference between the components of model A. It should be noted that both indented configurations were designed to have the same ratio of total volume to the

cube of the fuselage length. However, the nondimensional fuselage volume, of models A and B was about 23 percent and 11 percent, respectively, less than the nondimensional volume of the basic parabolic body of model C.

The pressure-drag or drag-rise coefficients of these models are given in figure 5(b). The comparison shows that the supersonic-area-rule design was more effective in reducing the pressure drag for the configuration with nacelles than for the corresponding configuration without nacelles at supersonic and transonic speeds. Both models A and B had the same average projected cross-sectional areas (figs. 3(b) and 3(d)) at $M = 1.41$; however, model A had about 16 percent less pressure drag at this design Mach number. The difference is brought out to show that average-area comparisons cannot be used for predicting the wave drag at supersonic speeds. As is shown in references 1 and 5, a detailed study of the projected-area distributions cut by Mach planes at each angle of roll of the configuration with respect to the Mach planes is required for predicting the pressure drag above Mach number 1.0. It appears that the lower pressure drag of model A over model B was due largely to a reduction in drag obtained by cancelling the wing cross-sectional areas in three spanwise places (about the nacelles and fuselage) instead of only about the body. This indicates that area-rule modifications should be made as close as possible to the sources of drag at supersonic speeds.

Of particular interest is the relative ΔC_D levels (fig. 5(b)) for Mach numbers at and slightly above 1.0. A visual comparison of the normal cross-sectional-area distributions (figs. 3(a) and 3(c)), according to the transonic area rule, does not explain the low drag rise of model A relative to the other models at $M = 1.0$. For example, one would expect the drag rise of model A to be slightly higher than model B because of the lower equivalent-body fineness ratio and more bumpy area distribution for model A. As a consequence, an attempt was made to explain these drag rises at Mach numbers slightly greater than 1.0 through application of the moment-of-area rule of reference 3. For configurations having symmetry in the wing plane, the moment-of-area rule states that the pressure drag at low supersonic speeds depends on both the longitudinal distribution of normal cross-sectional area and the second moment-of-area distribution (moment-of-inertia distribution). It can be shown from reference 3 that the drag coefficient resulting from the second moment is proportional to the peak value of $M_2(x)/l_2^4$ and a function of the relative bumpiness of the second moment distribution in comparison to the optimum area moment, just as the drag coefficient from the area distribution is proportional to the peak value of A/l^2 (or $(d/l)^2$ of the equivalent body) and a function of the relative shape of the area distribution in comparison to the optimum area distribution. As the Mach number approaches 1.0 the drag from the second moment approaches zero. Since the second moment-of-area distributions of the fuselage are negligible, only the moment-of-inertia distributions of the wing and wing with nacelles

need be compared (ref. 3). Such a comparison is given in figure 6(a) for both the actual second moment distributions and the optimumized versions of the second moments for models A, B, and C.

The nondimensionalized second moment-of-area distributions in figure 6(a) show that adding the nacelles greatly reduces the peak value of $M_2(x)/l_2^4$. This large reduction results from the added length of the moment distribution due to the nacelles which more than offsets the added moment from the nacelles; whereas, the changes in the peak values of A/l^2 (figs. 3(a) and 3(c)) seem to be far less significant. It appears, therefore, that the low pressure drag of model A relative to the other models was primarily due to the large reduction in the maximum value of the second moment in spite of the great departure from the optimum distribution.

In order to help substantiate the lower ΔC_D for model A at low supersonic speeds, the actual pressure drags are compared with the theoretical pressure drags of the optimumized versions of the second moment distributions in figure 6 and the normal cross-sectional-area distributions (not shown). The theoretical values of ΔC_D for the optimumized configurations were computed in the manner described in reference 3. The optimum pressure drags at low supersonic speeds are in the same relative order as the actual and indicate the savings in drag obtained from the designs employed for models A and B relative to model C. At $M = 1.0$, the theory shows a slightly greater ΔC_D for the optimumized version of model A over model B. The optimum distributions and pressure drags indicate that the design may be improved at these Mach numbers, but it has yet to be determined whether or not such optimumized distributions (according to the moment-of-area rule) also would give favorable results at higher supersonic speeds. It should be noted also that the nacelle indentation contributed to lowering the drag rise, for if the nacelles were not indented the peak values of the second moment and cross-sectional area of model A would be greater than for the present case.

Figure 7 shows an application of the transonic-area-rule concept (ref. 2) for predicting the sonic drag rise. Models D and E were duplicate equivalent bodies of revolution for the basic wing-body configuration (model C). The pressure drag of both equivalent bodies compares favorably with that from the basic configuration (model C) between the drag-rise Mach number and the speed of sound. At Mach number 1.0, the drag rise of these equivalent bodies is about 15 percent greater than that for model C.

CONCLUDING REMARKS

The supersonic-area-rule concept was found to be an effective guide of designing a straight-wing—body configuration with large symmetrically mounted nacelles for low pressure drag between Mach numbers 0.9 and 1.53. The pressure drag from the configuration with nacelles was significantly less than that from a corresponding configuration without nacelles throughout the speed range. Both configurations were designed to have the same average area distribution at Mach number 1.41. The moment-of-area rule was useful in explaining the relative drag rises of the models at low supersonic speeds.

The pressure drag from the Mach number 1.0 equivalent bodies of revolution compared favorably with that from the corresponding straight-wing—body configuration between the drag-rise Mach number and the speed of sound.

Langley Aeronautical Laboratory,
National Advisory Committee for Aeronautics,
Langley Field, Va., February 17, 1956.

REFERENCES

1. Jones, Robert T.: Theory of Wing-Body Drag at Supersonic Speeds. NACA RM A53H18a, 1953.

2. Whitcomb, Richard T.: A Study of the Zero-Lift Drag-Rise Characteristics of Wing-Body Combinations Near the Speed of Sound. NACA RM L52H08, 1952.

3. Baldwin, Barrett S., Jr., and Dickey, Robert R.: Application of Wing-Body Theory to Drag Reduction at Low Supersonic Speeds. NACA RM A54J19, 1955.

4. Hopko, Russell N., Piland, Robert O., and Hall, James R.: Drag Measurements at Low Lift of a Four-Nacelle Airplane Configuration Having a Longitudinal Distribution of Cross-Sectional Area Conducive to Low Transonic Drag Rise. NACA RM L53E29, 1953.

5. Hoffman, Sherwood, Wolff, Austin L., and Faget, Maxime A.: Flight Investigation of the Supersonic Area Rule for a Straight Wing-Body Configuration at Mach Numbers Between 0.8 and 1.5. NACA RM L55C09, 1955.

6. Hoffman, Sherwood: A Flight Investigation of the Transonic Area Rule for a 52.5° Sweptback Wing-Body Configuration at Mach Numbers Between 0.8 and 1.6. NACA RM L54H13a, 1954.

7. Robinson, Harold L.: A Transonic Wind-Tunnel Investigation of the Effects of Body Indentation, As Specified by the Transonic Drag-Rise Rule, on the Aerodynamic Characteristics and Flow Phenomena of a 45° Sweptback-Wing—Body Combination. NACA RM L52L12, 1953.

8. Williams, Claude V.: A Transonic Wind-Tunnel Investigation of the Effects of Body Indentation, As Specified by the Transonic Drag-Rise Rule, on the Aerodynamic Characteristics and Flow Phenomena of an Unswept-Wing—Body Combination. NACA RM L52L23, 1953.

9. Wornom, Dewey E., and Osborne, Robert S.: Effects of Body Indentation on the Drag Characteristics of a Delta-Wing—Body Combination at Transonic Speeds. NACA RM L54K12a, 1955.

10. Carlson, Harry W.: Preliminary Investigation of the Effects of Body Contouring As Specified by the Transonic Area Rule on the Aerodynamic Characteristics of a Delta Wing-Body Combination at Mach Numbers of 1.41 and 2.01. NACA RM L53G03, 1953.

11. Holdaway, George H.: Comparison of Theoretical and Experimental Zero-Lift Drag-Rise Characteristics of Wing-Body-Tail Combinations Near the Speed of Sound. NACA RM A53H17, 1953.

12. Alksne, Alberta.: A Comparison of Two Methods for Computing the Wave Drag of Wing-Body Combinations. NACA RM A55A06a, 1955.

13. Hoffman, Sherwood: An Investigation of the Transonic Area Rule by Flight Tests of a Sweptback Wing on a Cylindrical Body With and Without Body Indentation Between Mach Numbers 0.9 and 1.8. NACA RM L53J20a, 1953.

14. McDevitt, John B.: An Experimental Investigation of Two Methods for Reducing Transonic Drag of Swept-Wing and Body Combinations. NACA RM A55B21, 1955.

15. Byrd, Paul F.: Theoretical Pressure Distributions for Some Slender Wing-Body Combinations at Zero Lift. NACA RM A54J07, 1955.

16. Whitcomb, Richard T.: Recent Results Pertaining to the Application of the "Area Rule." NACA RM L53I15a, 1953.

17. Whitcomb, Richard T., and Fischetti, Thomas L.: Development of a Supersonic Area Rule and an Application to the Design of a Wing-Body Combination Having High Lift-to-Drag Ratios. NACA RM L53H31a, 1953.

18. Lomax, Harvard, and Heaslet, Max. A.: A Special Method for Finding Body Distortions That Reduce the Wave Drag of Wing and Body Combinations at Supersonic Speeds. NACA RM A55B16, 1955.

19. Hall, James Rudyard: Comparison of Free-Flight Measurements of the Zero-Lift Drag Rise of Six Airplane Configurations and Their Equivalent Bodies of Revolution at Transonic Speeds. NACA RM L53J21a, 1954.

20. Hoffman, Sherwood, and Robins, A. Warner: Drag of Canopies at Transonic and Supersonic Speeds. NACA RM L55I23, 1956.

21. Morrow, John D., and Nelson, Robert L.: Large-Scale Flight Measurements of Zero-Lift Drag of 10 Wing-Body Configurations at Mach Numbers From 0.8 to 1.6. NACA RM I52D18a, 1953.

22. Wallskog, Harvey A., and Hart, Roger G.: Investigation of the Drag of Blunt-Nosed Bodies of Revolution in Free Flight at Mach Numbers From 0.6 to 2.3. NACA RM L53D14a, 1953.

23. Van Driest, E. R.: Turbulent Boundary Layer in Compressible Fluids. Jour. Aero. Sci., vol. 18, no. 3, Mar. 1951, pp. 145-160, 216.

TABLE I.- COORDINATES OF NACA 65A004.5 AIRFOIL

Station, percent chord	Ordinate, percent chord
0	0
.5	.349
.75	.424
1.25	.540
2.50	.738
5.0	.986
7.5	1.194
10	1.368
15	1.646
20	1.855
25	2.014
30	2.131
35	2.208
40	2.246
45	2.245
50	2.196
55	2.099
60	1.957
65	1.780
70	1.572
75	1.338
80	1.084
85	.818
90	.549
95	.280
100	.010
L.E. radius: 0.130 percent chord T.E. radius: 0.0115 percent chord	

TABLE II.- COORDINATES OF BODY INDENTED

FOR WING AND NACELLE

[Stations measured from body nose]

Station, in.	Ordinate, in.
0	0
.769	.188
1.538	.370
3.077	.710
4.615	1.021
7.692	1.553
9.231	1.775
10.769	1.940
12.308	2.055
13.846	2.147
15.385	2.227
16.923	2.275
18.462	2.287
20.000	2.275
21.538	2.271
23.077	2.185
24.615	2.047
26.154	1.919
27.692	1.798
29.231	1.691
30.769	1.598
32.308	1.511
33.846	1.442
35.385	1.430
36.923	1.445
38.462	1.476
40.000	1.494
41.538	1.490
43.077	1.458
44.615	1.392
46.154	1.288
47.692	1.192
49.231	1.119
50.000	1.087

TABLE III.- COORDINATES OF INDENTED NACELLE

[Stations measured from nacelle inlet]

Station, in.	Ordinate, in.
0	0.910
.302	.991
.446	1.021
.662	1.064
1.020	1.131
1.379	1.188
1.538	1.215
3.077	1.368
4.615	1.400
6.154	1.394
7.692	1.373
9.231	1.339
10.769	1.304
12.308	1.291
13.846	1.324
15.385	1.324
16.923	1.302
18.462	1.237
20.000	1.127
21.920	.934

Inside diameter = 0.910 in.

TABLE IV.- COORDINATES OF BODY INDENTED FOR WING

[Stations measured from body nose]

Station, in.	Ordinate, in.
0	0
1	.245
2	.481
4	.923
6	1.327
10	2.019
14	2.558
18	2.942
22	3.173
30	3.233
32	3.160
34	2.920
36	2.650
38	2.375
40	2.185
42	2.095
44	2.108
46	2.185
48	2.272
50	2.348
52	2.402
54	2.375
56	2.285
58	2.149
60	2.007
62	1.857
64	1.698
65	1.615

TABLE V.- COORDINATES OF BASIC PARABOLIC BODY

[Stations measured from body nose]

Station, in.	Ordinate, in.
0	0
2	.490
4	.962
8	1.846
12	2.654
20	4.038
28	5.116
36	5.884
44	6.346
52	6.500
60	6.466
68	6.362
76	6.190
84	5.950
92	5.640
100	5.262
108	4.814
116	4.298
124	3.714
130	3.230

TABLE VI.- COORDINATES OF EQUIVALENT BODY OF REVOLUTION FOR BASIC WING-BODY COMBINATION

[Stations measured from body nose]

Station, in.	Ordinate, in.
0	0
.308	.074
.923	.204
1.538	.311
2.154	.394
2.769	.453
3.385	.488
4.000	.500
4.615	.497
5.080	.492
5.216	.497
5.453	.516
5.750	.546
5.927	.564
6.164	.586
6.342	.594
6.638	.588
6.935	.554
7.231	.502
7.527	.432
7.823	.399
8.308	.370
8.923	.331
9.538	.286
9.846	.261
10.000	.248

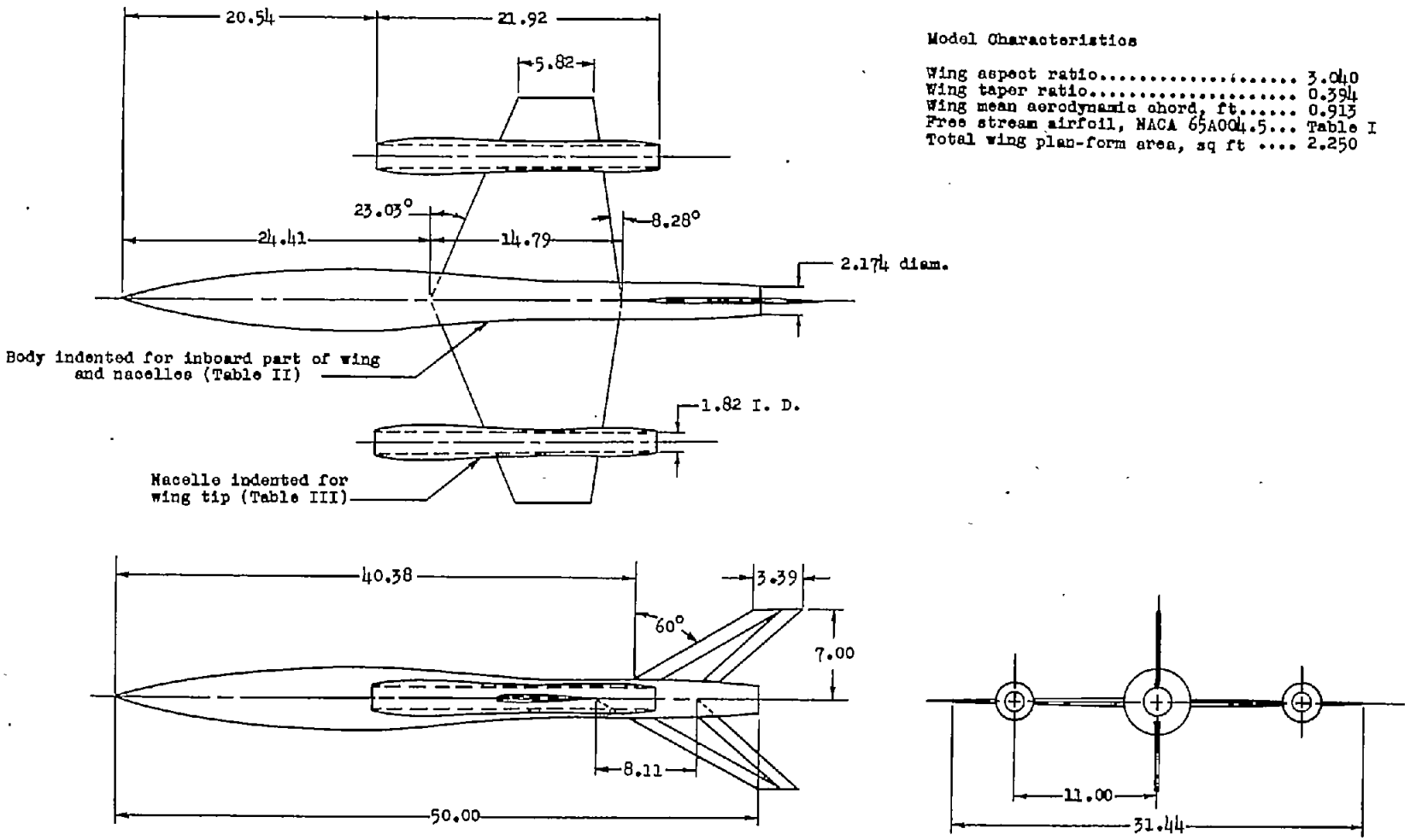

(a) Wing-body-nacelle configuration designed for M = 1.41. Model A.

Figure 1.- Details and dimensions of models. All dimensions are in inches.

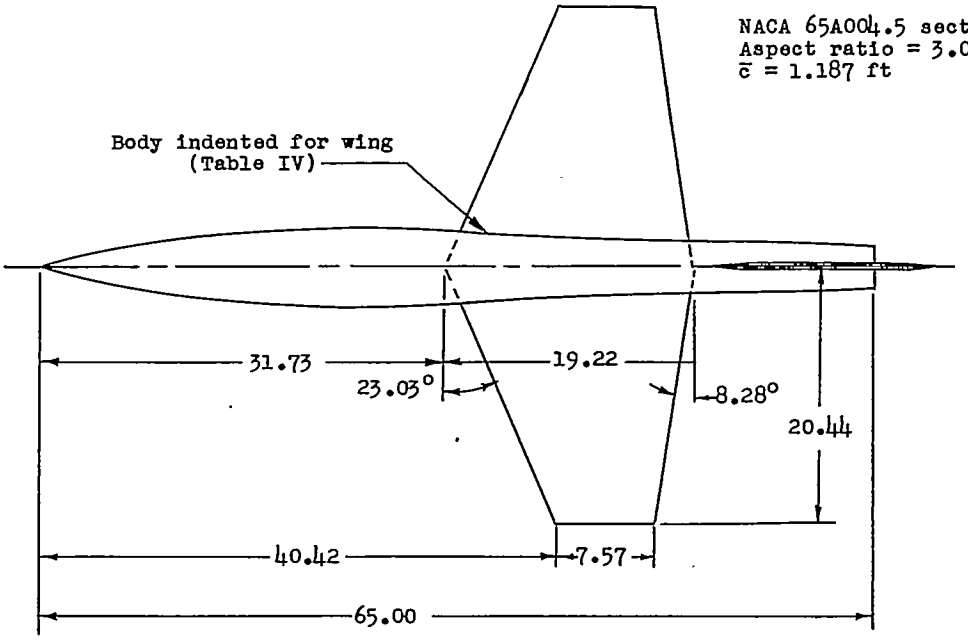

(b) Wing-body configuration designed for M = 1.41 (ref. 5). Model B.

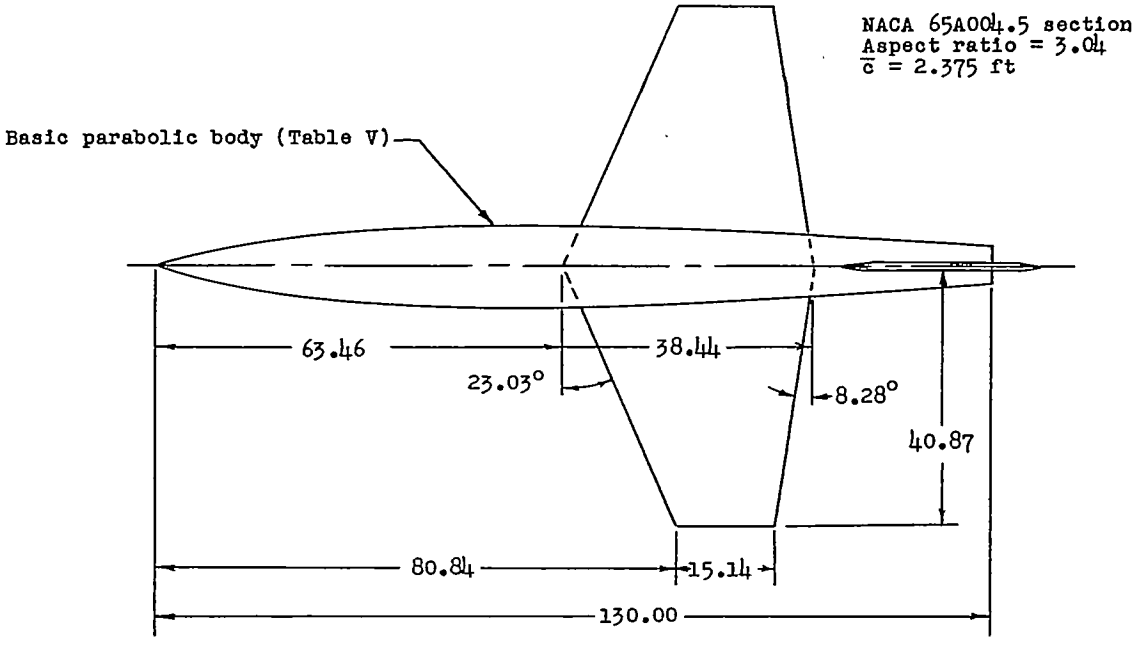

(c) Basic wing-body configuration (ref. 21). Model C.

Figure 1.- Continued.

[redacted]

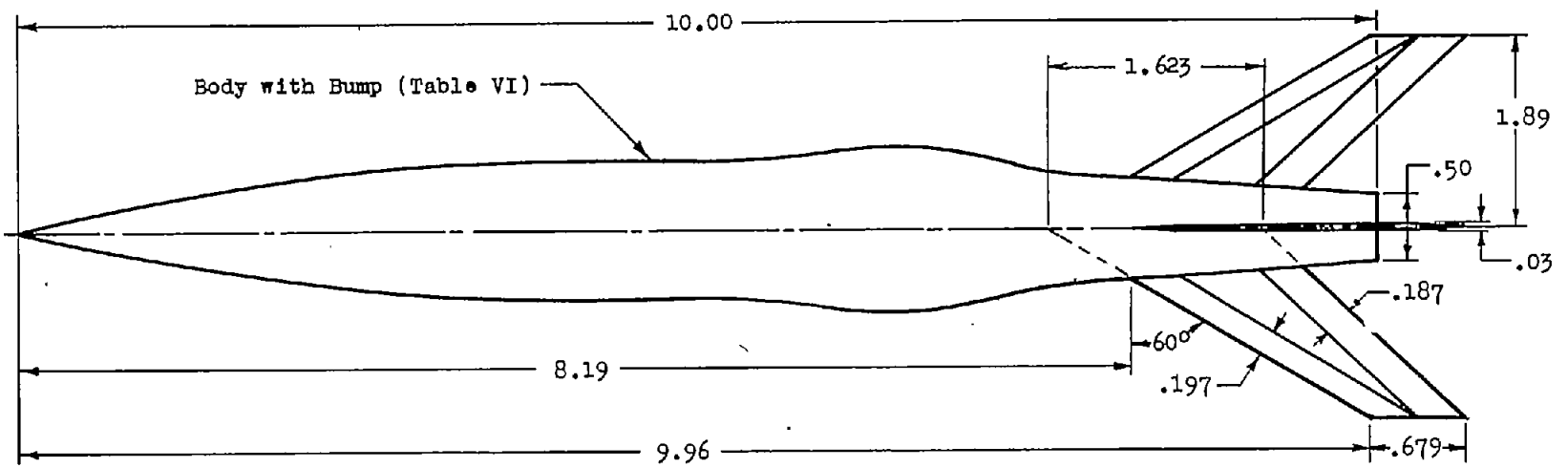

(d) Equivalent body of revolution (M = 1.0) for basic wing-body configuration. Models D and E.

Figure 1.- Concluded.

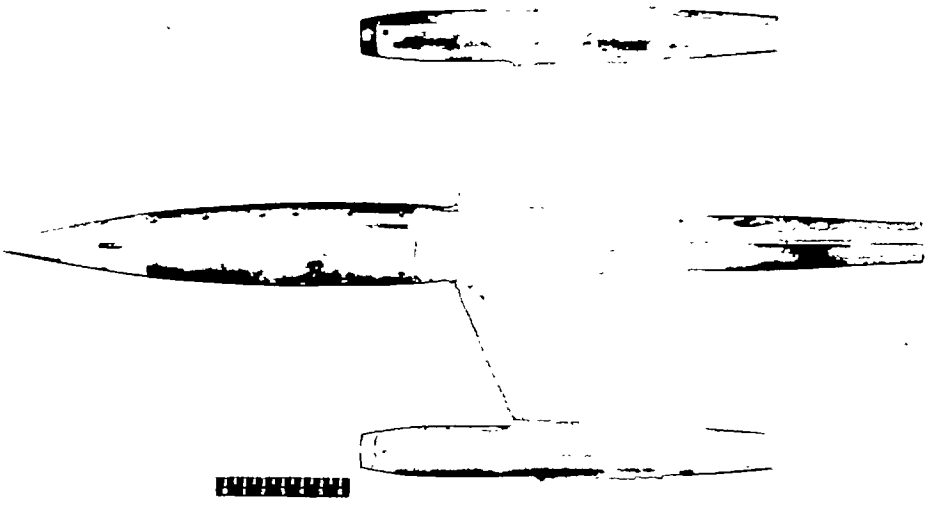

(a) Top view. Model A. L-89495.1

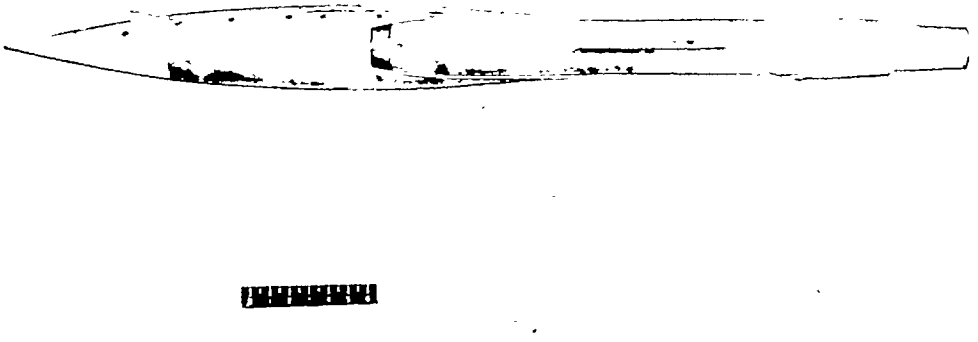

(b) Side view. Model A. L-89496.1

Figure 2.- Photographs of models.

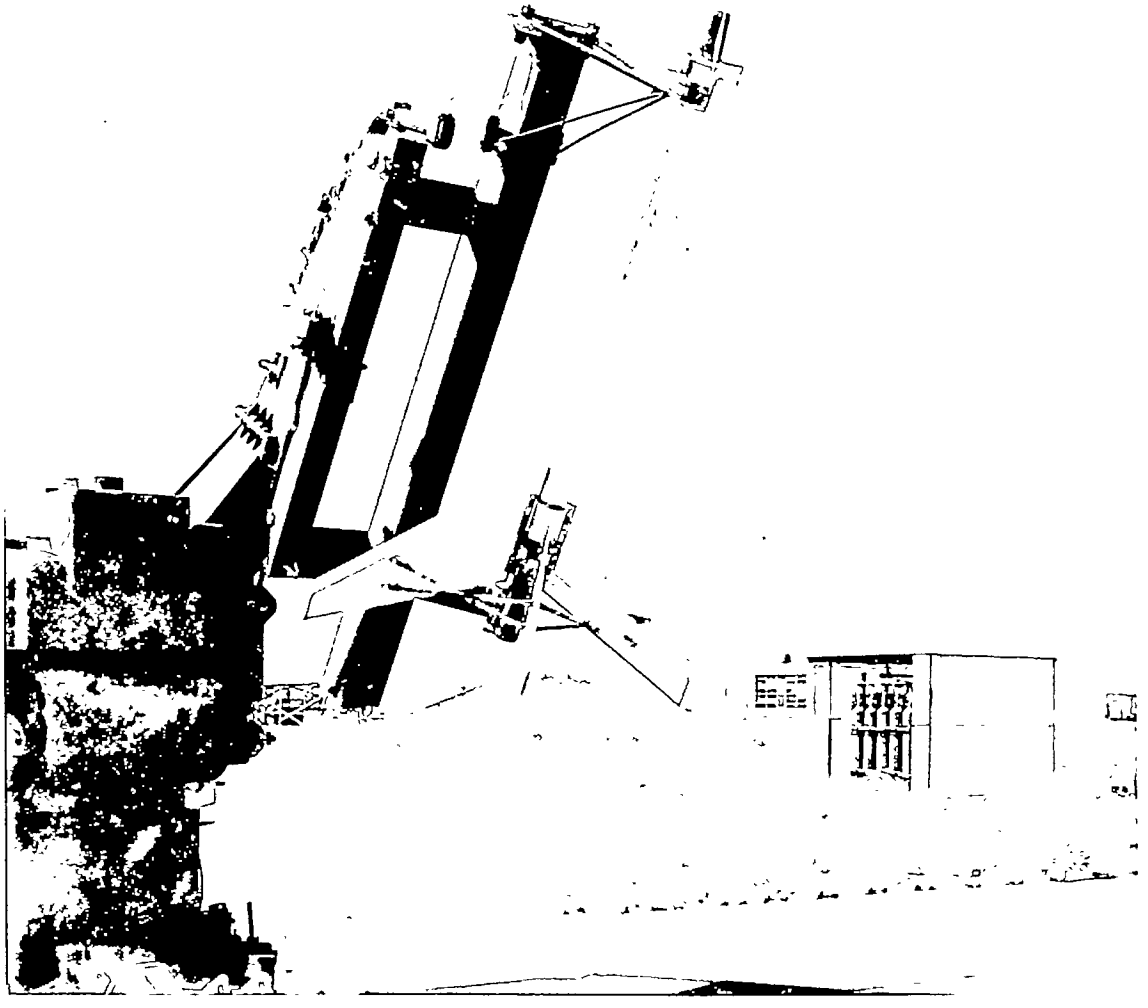

(c) Model A on zero-length launcher. L-89646

Figure 2.- Concluded.

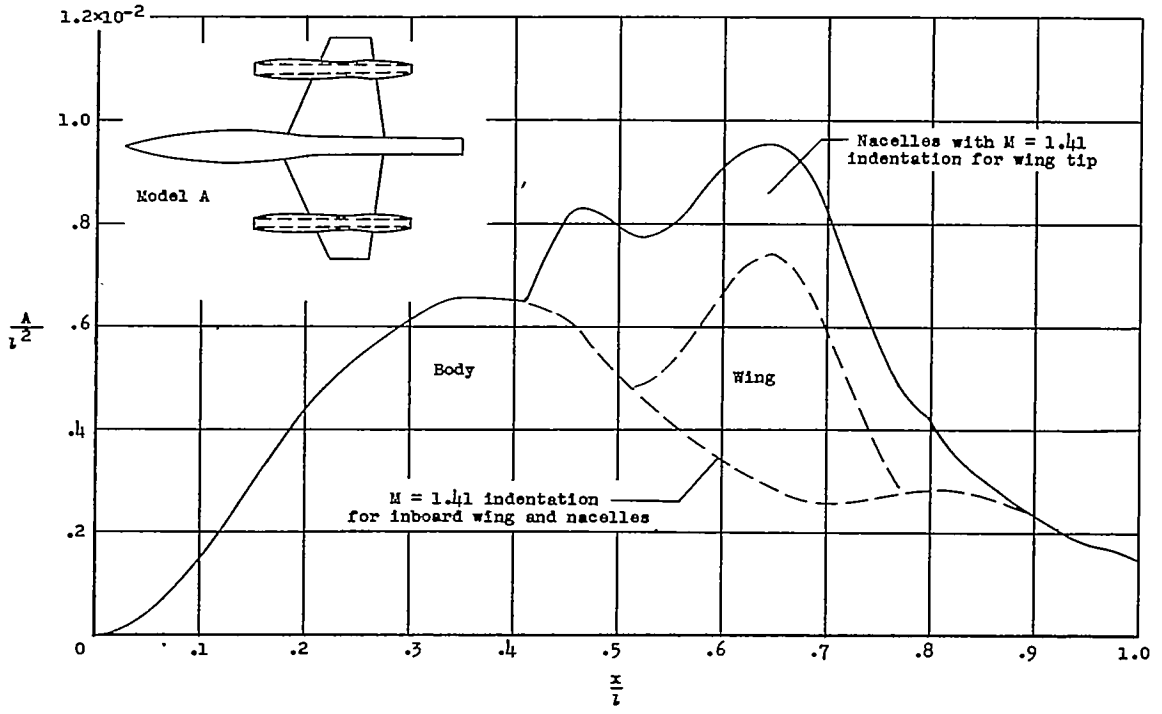

(a) Normal area distribution for M = 1.0. Model A.

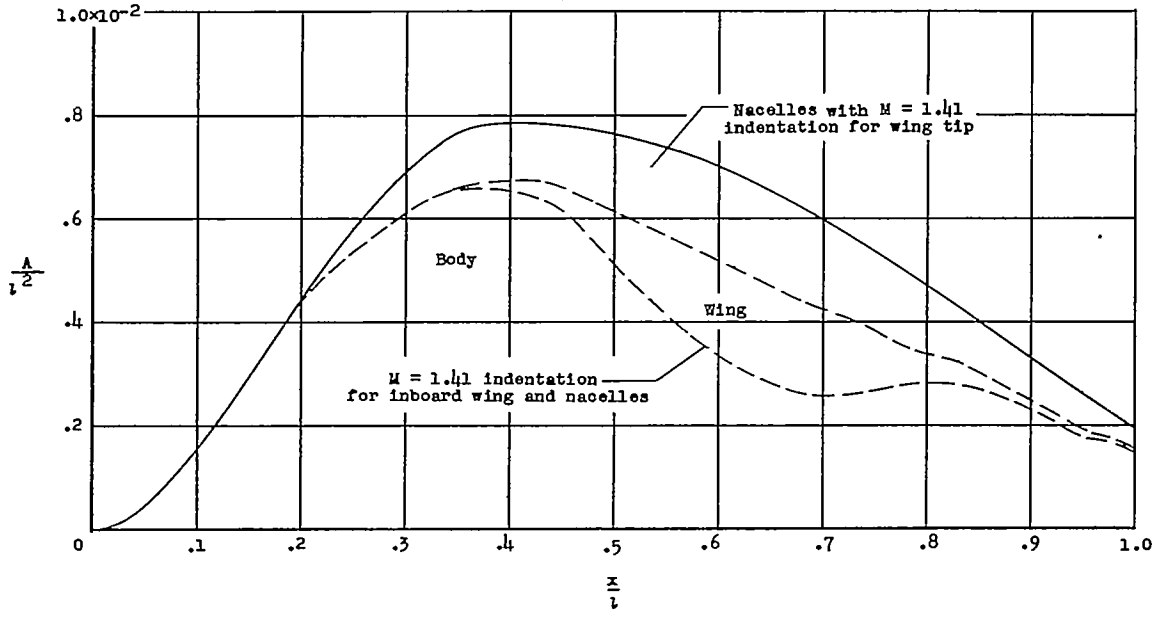

(b) Average area distribution for M = 1.41. Model A.

Figure 3.- Comparison of area distributions of models.

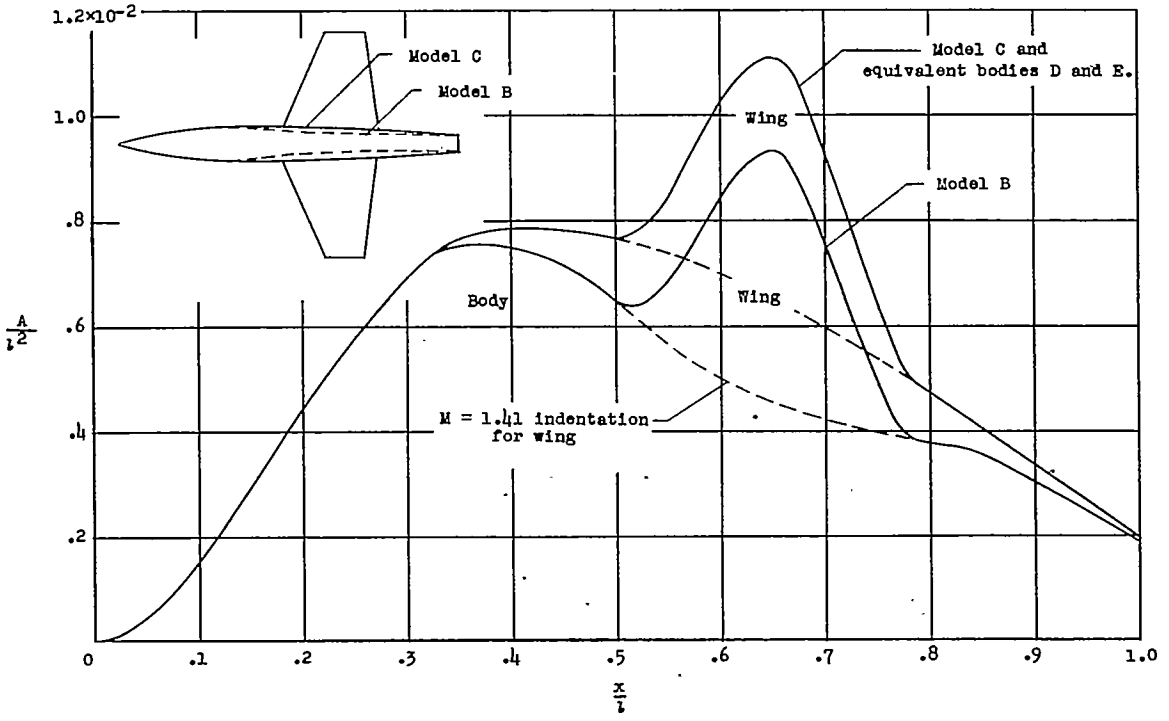

(c) Normal area distributions for M = 1.0. Models B, C, D, and E.

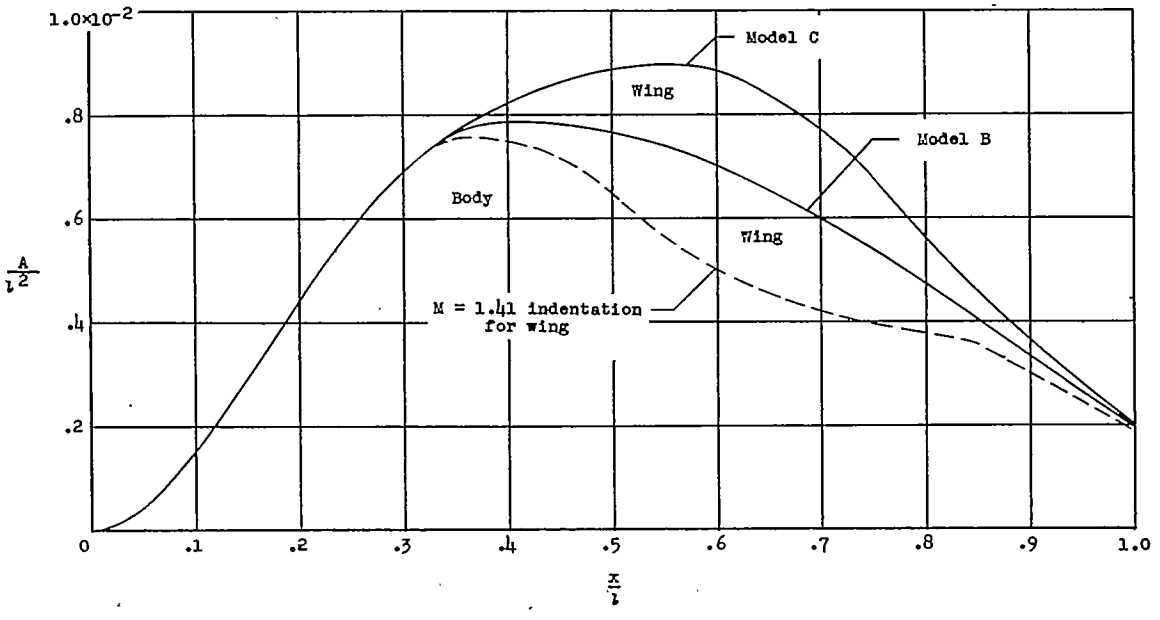

(d) Average area distributions for M = 1.41. Models B and C.

Figure 3.- Concluded.

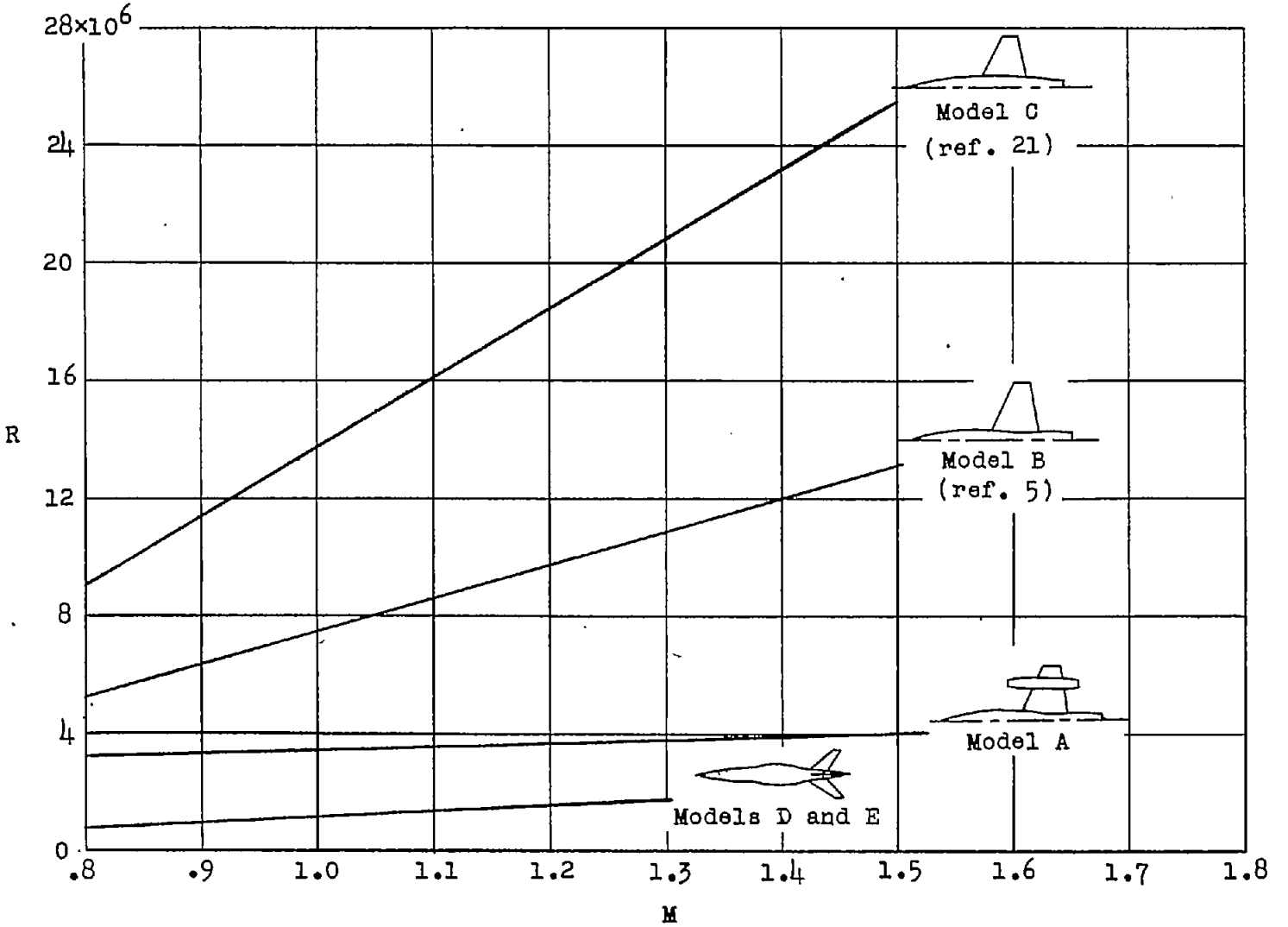

Figure 4.- Variation of Reynolds number with Mach number. Reynolds number is based on mean aerodynamic chord of wing.

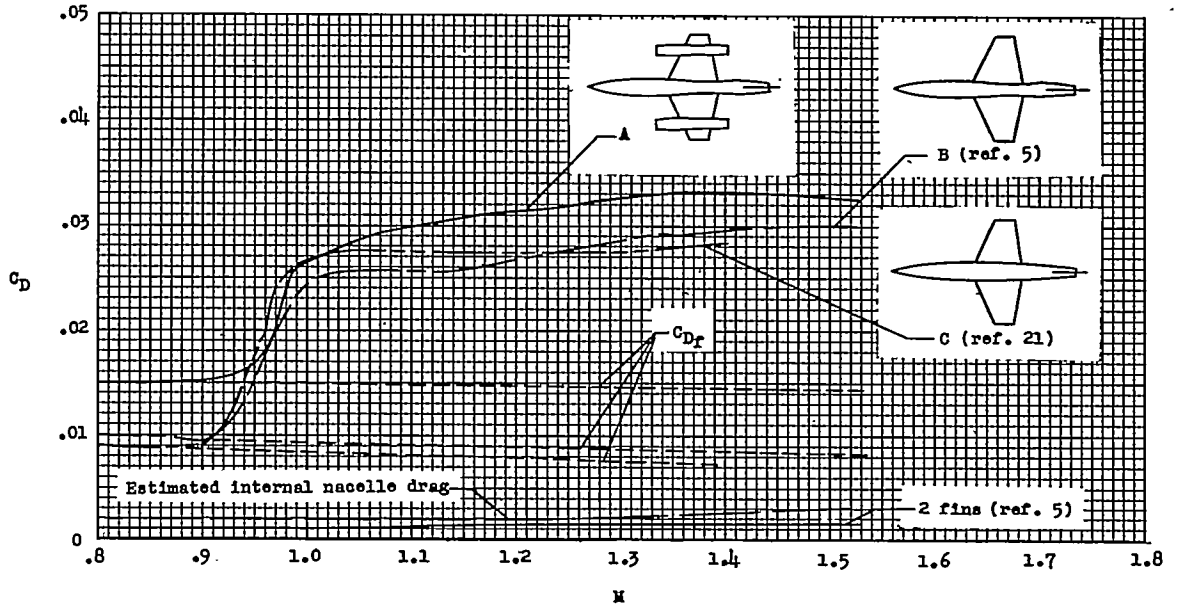

(a) Total drag.

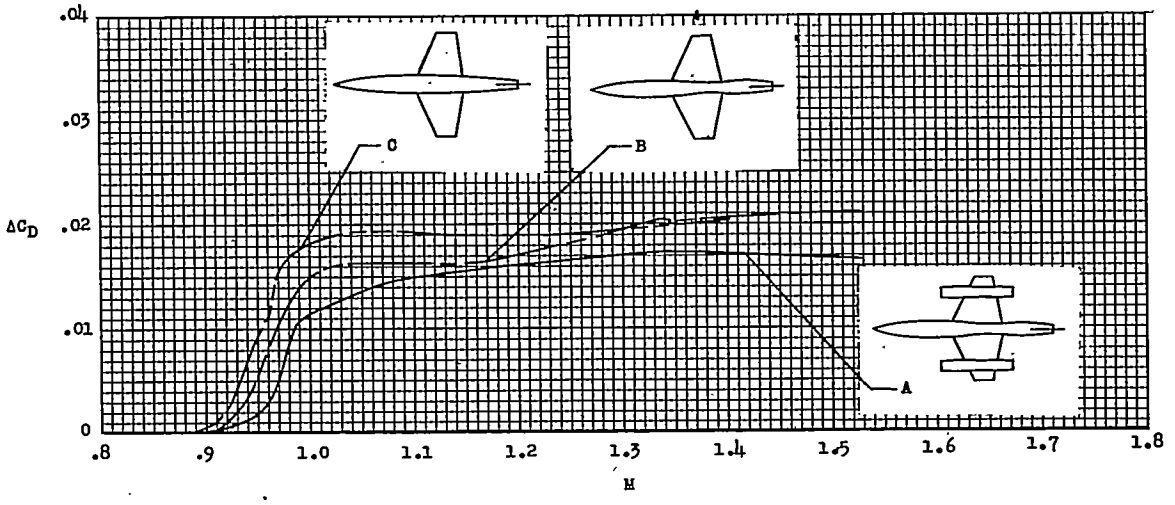

(b) Pressure drag.

Figure 5.- Comparisons of drag coefficients of models A, B, and C.

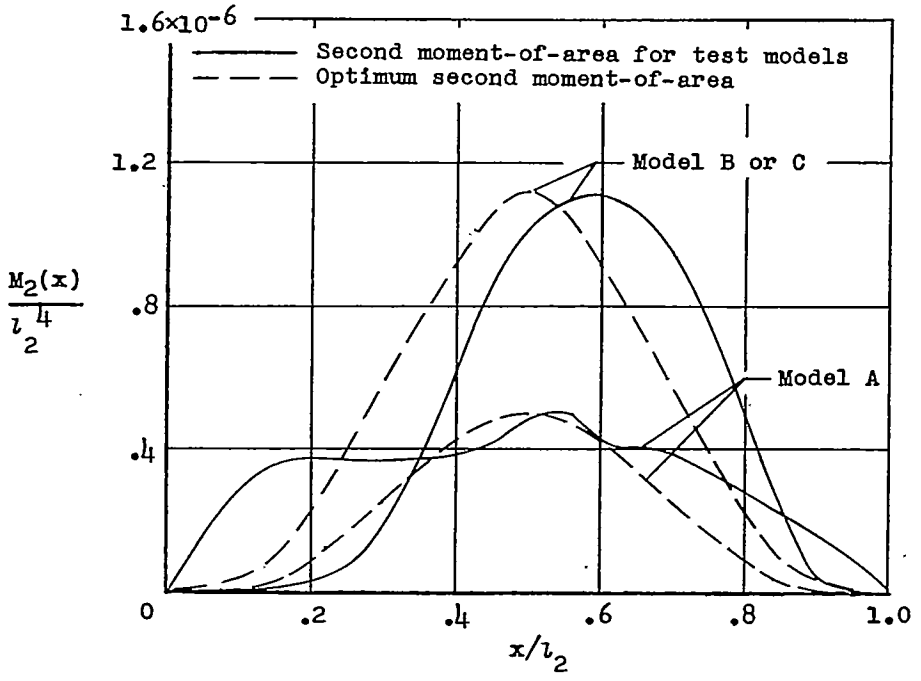

(a) Nondimensionalized area moment of inertia distribution.

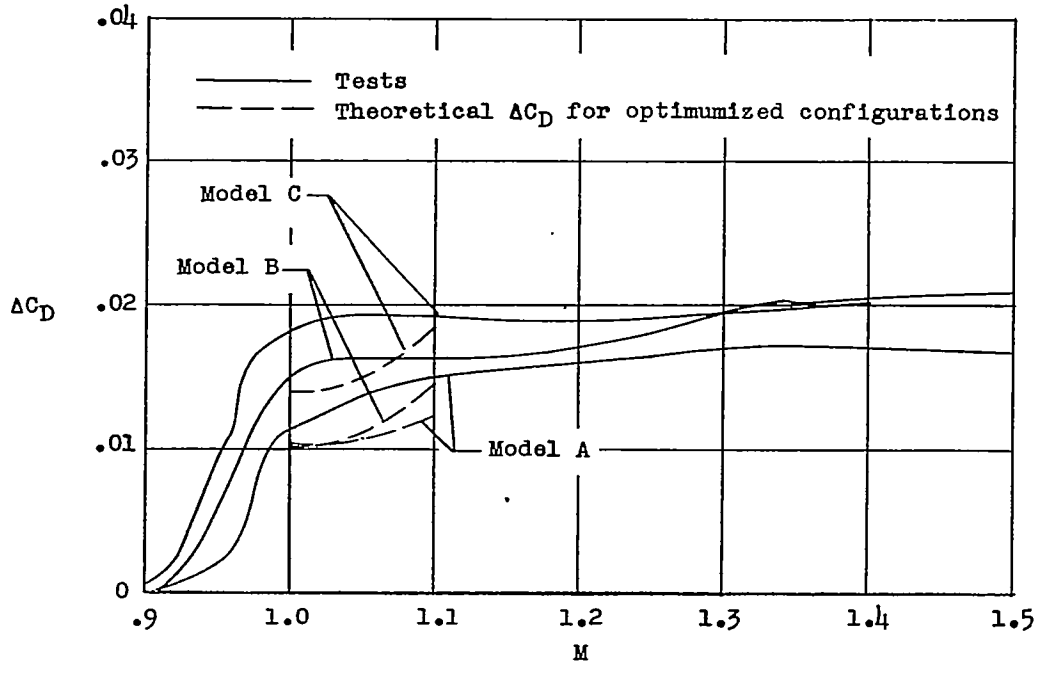

(b) Pressure drag.

Figure 6.- Comparisons of area moment of inertia distributions and pressure drags for test models and comparable optimumized configurations.

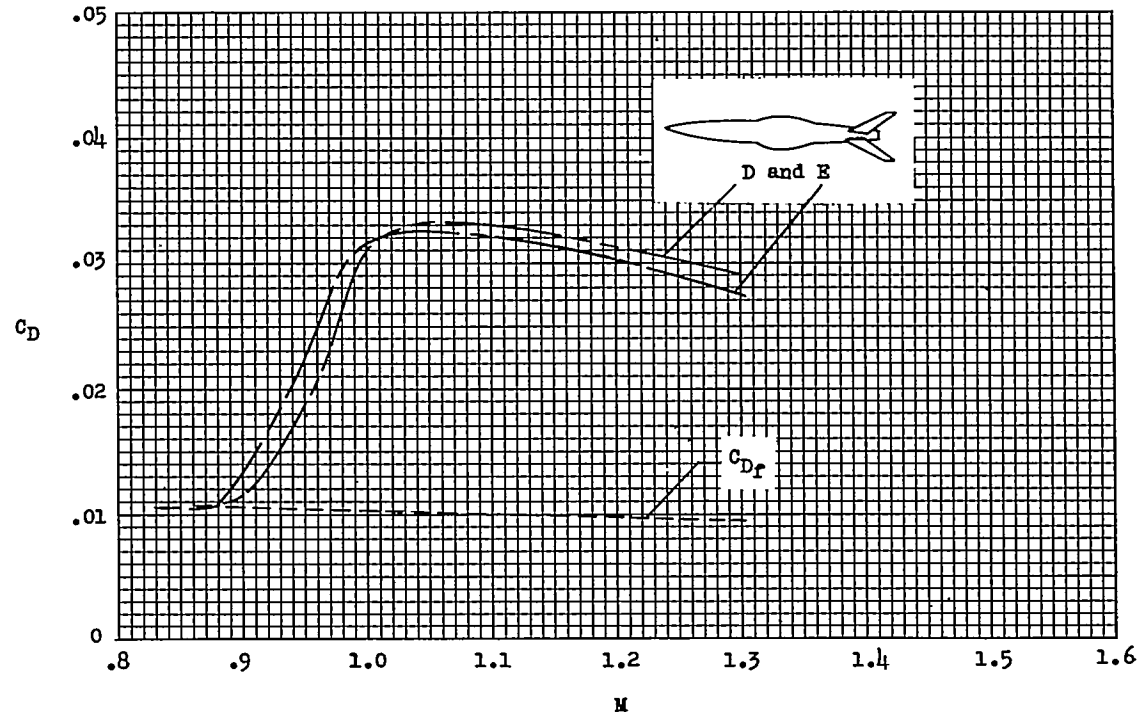

(a) Total drag.

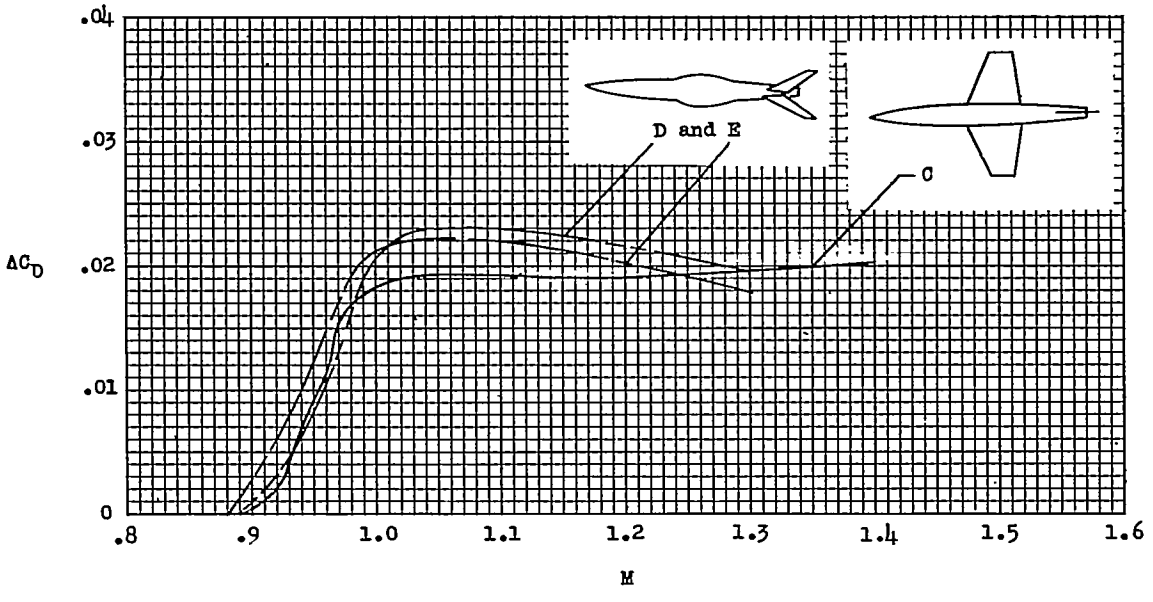

(b) Pressure drag.

Figure 7.- Comparisons of drag coefficients of models C, D, and E.